ARTICLE

Identification of Superoxide O_2^- during Thermal Decomposition of Molten KNO_3-$NaNO_2$-$NaNO_3$ Salt by Electron Paramagnetic Resonance and UV-Vis Absorption Spectroscopy

Shu-ting Liu, Tao Su*, Peng Zhang, Ze-jie Fei, Hong-tao Liu*

Department of Molten Salt Chemistry and Engineering, Shanghai Institute of Applied Physics, Chinese Academy of Sciences, Shanghai 201800, China

(Dated: Received on March 21, 2017; Accepted on June 20, 2017)

On account of excellent thermal physical properties, molten nitrates/nitrites salt has been widely employed in heat transfer and thermal storage industry, especially in concentrated solar power system. The thermal stability study of molten nitrate/nitrite salt is of great importance for this system, and the decomposition mechanism is the most complicated part of it. The oxide species O_2^{2-} and O_2^- were considered as intermediates in molten KNO_3-$NaNO_3$ while hard to been detected in high temperature molten salt due to their trace concentration and low stability. In this work, the homemade *in situ* high temperature UV-Vis instrument and a commercial electron paramagnetic resonance were utilized to supply evidence for the formation of superoxide during a slow decomposition process of heat transfer salt (HTS, 53 wt% KNO_3/40 wt% $NaNO_2$/7 wt% $NaNO_3$). It is found that the superoxide is more easily generated from molten $NaNO_2$ compared to $NaNO_3$, and it has an absorption band at 420−440 nm in HTS which red shifts as temperature increases. The band is assigned to charge-transfer transition in NaO_2 or KO_2, responsible for the yellow color of the molten nitrate/nitrite salt. Furthermore, the UV absorption bands of molten $NaNO_2$ and $NaNO_3$ are also obtained and compared with that of HTS.

Key words: Superoxide, Decomposition of heat transfer salt, High temperature UV-visible, Electron paramagnetic resonance

I. INTRODUCTION

Concentrated solar power (CSP) uses molten salt as thermal energy storage (TES) and heat transfer fluid (HTF) medium, which have high energy density and high stability compared to photovoltaic or wind powers. CSP is gaining increasing interest and has become one of the most promising new energy technologies [1, 2]. Molten nitrates/nitrites salt has been widely used for HTF and TES on account of their high working temperatures, good fluidity and heat storage capacity, relatively low vapor pressure and corrosion, and other good thermal physical properties [3−6]. Two important nitrates/nitrites based molten salt mixtures have been employed in CSP plants: solar salt, an eutectic binary salt of 60 wt% $NaNO_3$-40 wt% KNO_3, melted at 221 °C and kept liquid at 288 °C in an insulated storage tank; and HTS (heat transfer salt or Hitec), an eutectic ternary salt of 40 wt% $NaNO_2$/7 wt% $NaNO_3$/53 wt% KNO_3, operating beyond its melting point of 142 °C [7−9]. Although solar salt and HTS have many merits, the thermal stability at the long term plays an important role in the running period of CSP system [10]. Generally, thermal stability involves the decomposition of every single component, and the mechanism is very complicated.

This is a consensus that HTS is much more unstable than solar salt at high temperature because of the low thermal decomposition temperature of sodium nitrite. Solar salt is commonly believed to be stable under 600 °C. While for Hitec/HTS, Alexander and Hindin [11] found it should be stable under 450 °C. Kearney *et. al.* [5] showed that its thermal stability temperature could be up to 535 °C. While Peng and coworkers [12] suggested that the upper operating temperature of HTS was about 500 °C under air atmosphere. Olivares's study [13] showed the stability changes in different atmosphere. Discrepancy comes that the same precise experimental conditions is hard to carry, as the decomposition will be affected by air, moisture, impurities and materials of container. Generally, the researchers identify the decomposition temperature by the macroscopic variations, such as the turning point on the curve of thermogravimetric (TG), appearance of endothermic peak in differential scanning calorimetry (DSC) measurement, rapid gas emitting in mass spectrum (MS)

*Authors to whom correspondence should be addressed. E-mail: liuhongtao@sinap.ac.cn

DOI:10.1063/1674-0068/30/cjcp1703046

measurement *etc.* Also, the decomposition reaction equations were speculated from the final products.

For $NaNO_2$, between 330 and 380 °C, the reaction sequence is proposed to be as follows [14−16]:

$$2NaNO_2 \triangleq Na_2O + NO\uparrow + NO_2\uparrow \quad (1)$$

$$NaNO_2 + 2NO \triangleq 2NaNO_3 + N_2\uparrow \quad (2)$$

$$Na_2O + 2NO_2 \triangleq NaNO_3 + NaNO_2\uparrow \quad (3)$$

$$NaNO_2 + NO_2 \triangleq NaNO_3 + NO\uparrow \quad (4)$$

Previous studies showed that the hyperoxides could be stabilized by interaction with the solution species such as alkali cations in molten nitrate salt [17]. Furthermore, Freeman [18] attributed the evolution of N_2 to the formation of superoxide which later decomposes to Na_2O and O_2 at higher temperatures. This view is also supported by Bond and Jacobs [19], they promoted a possible equation

$$2NO_2^- \rightarrow N_2 + 2O_2^- \quad (5)$$

For $NaNO_3$, it is widely believed that the first stage of decomposition [14−16] is

$$2NaNO_3 \triangleq 2NaNO_2 + O_2\uparrow \quad (6)$$

Kust *et al.* [16] demonstrated that the NO_2 in alkali metal nitrate can be detected at temperature as low as 295 °C. Nissen and Meeker [20] monitored the concentration of NO_2 in solar salt at 550−600 °C with different oxygen partial pressures. It was found that the percentage of nitrite ion increased with the rising of temperature and the decrease of oxygen partial pressure. In addition, the oxide species, O^{2-}, O_2^{2-} or O_2^-, were unable to be detected in their experiments and their concentrations could be less than 10^{-5} mol/kg, which are below the detection limit of the pH measurements. However, Zambonin's studies [21−23] showed the oxide species were produced in molten $NaNO_3$-$NaNO_3$, as follows:

$$O^{2-} + NO_3^- NO_2^- + O_2^{2-} \quad (7)$$

$$O_2^{2-} + 2NO_3^- \rightleftharpoons 2NO_2^- + 2O_2^- \quad (8)$$

$$O_2^{2-} + O_2 \rightleftharpoons 2O_2^- \quad (9)$$

Eqs.(7), (8) and (9) existed with equilibrium constants of $K_7 \approx 3$, $K_8 \approx 6.7\times10^{-11}$ and $K_9 \approx 3.5\times10^5$ all at 229 °C by electrochemical method. Afterwards, in view of the paramagnetism of O_2^-, Zambonin [24] used electron paramagnetic resonance (EPR) to detect the signal of O_2^- in the quenched $NaNO_3$-KNO_3 salt. The signal was still detected after preserving in inert atmosphere for months, which implies that O_2^- can exist in the binary nitrate salts under room temperature. Nevertheless, the *in situ* probe on O_2^- in molten ternary nitrates/nitrites salt (HTS) was never performed, and the way of superoxide anion generation in molten nitrates salt is still undeterminable.

Generally, many analytical methods [25] are able to be used to identify O_2^-, for instance, EPR [26], Raman [27], UV-visible [28−31] and IR [32] spectroscopic methods, *etc.* However, the spectral detection of O_2^- is hard to carry out because of its low concentration and high reactivity in high temperature molten salt, especially, for *in situ* probe. Although UV-visible, IR absorption and Raman spectroscopy instruments have been used to study the spectra of high temperature molten nitrates/nitrites salt [33−35], the results did not show a spectral evidence for the presence of O_2^-. While by adding KO_2 into FLiNaK (LiF/NaF/KF, 46.5 mol%/11.5 mol%/45 mol%), Young and coworkers [36] observed an absorption peak at 254 nm which was assigned to O_2^- by subtracting origin absorption spectrum of molten FLiNaK at 500 °C. This peak quickly disappeared afterwards. Alkali metal superoxide presents yellow. And the higher the temperature, the deeper the color. So it is very likely that superoxide ion can be discerned by visible absorption spectra in molten alkali metal salt if it really exists.

In this work, the high temperature UV-visible absorption spectrometer was built, by which decomposition mechanism of the molten HTS salt was investigated. In this process, it mainly was involving production and identification of O_2^-. Additionally, EPR experiment was also carried out to further verify the conclusion from UV-visible absorption spectroscopy.

II. EXPERIMENTS

A. Sample preparation

$NaNO_3$, $NaNO_2$, KNO_3 (AR) and KO_2 (>96.5% pure) obtained from Sinopharm Chemical Reagent Co., Ltd. $NaNO_3$ and KNO_3 are pure white crystals while $NaNO_2$ is slightly yellow crystals, KO_2 is golden yellow powder. All reagents are placed into the glovebox to avoid air and moisture due to the hygroscopicity of solid salts and strong reactivity of superoxide. Besides, the samples will be sealed during transfer.

The procedure of HTS preparation includes three steps. Firstly, drying operation at 120 °C on three components ($NaNO_3$, $NaNO_2$, and KNO_3) was conducted for two days to eliminate the potential free water. Secondly, three components were weighed by proportion of 7 wt%, 40 wt%, and 53 wt% and placed into vitreous carbon crucible for grounding uniformly, after that, they were heated to 120 °C for 10 h in furnace to reeliminate the free water, Thirdly, it keeps the temperature at 250 °C for 24 h, three components can form the eutectic salt (HTS). Finally, after the eutectic salt was cooled, it was transferred to glovebox. The prepared molten salt was sampled to perform the differential scanning calorimetry (DSC) test to verify its quantity. The result was shown in FIG. 1, from which the melting point can be determined to be 142.9 °C that is

DOI:10.1063/1674-0068/30/cjcp1703046

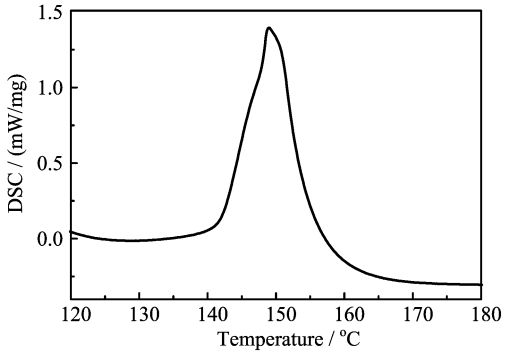

FIG. 1 DSC result of HTS samples.

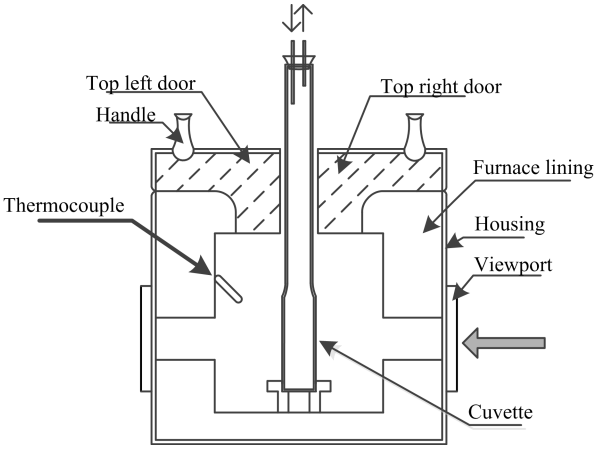

FIG. 2 The overview of furnace for high temperature UV-visible absorption spectroscopy.

in good agreement with the authentic one.

B. Ultraviolet-visible absorption spectroscopy

Owing to no standard instrument competent for the high temperature measurement of molten salts, a UV-visible spectrometer was built to obtain molten salts *in situ* absorption spectra at high temperature.

The system includes three main components, the light source, furnace, and a fiber spectrometer. The light source is deuterium lamp with iDH2000-UV bought from Shanghai Ideaoptics Corp., Ltd. that is connected with one fiber. The apparatus scheme of furnace is displayed in FIG. 2.

The cover of furnace is two-half pattern with a hole of diameter 20 mm in the center and four windows are situated on the opposition and same level position that can allow the light beam to pass through. A metal base is located at the bottom of the furnace hearth that can be used to orientate the cuvette. A temperature controller connected with the furnace provided both the actual temperature readout and the means for setting the target temperature with actual power control. The light goes straightly through the furnace to the fiber linked with the spectrometer of QE pro 65 bought from Ocean Optics.

The spectrometer is controlled by a computer, on which the processed real-time spectrum is recorded. In addition, the sample cell is a modified quartz cuvette welded a long tube of 15 cm, which is designed to allow the tube mouth out of the furnace hearth and away from high temperature, so that the routine seal methods can be adopted. For example, a rubber plug or rubber membrane can be used to seal the cuvette. In the experiment, it was found that a closed system isolated from air can be obtained using these routine seal methods. Procedures to obtain the spectra are described here. Firstly, the empty cuvette was employed to get the background. After that, the sample was loaded into cuvette in glovebox and then sealed by the rubber membrane which can relieve the increased pressure caused by the slow gas emission from molten salt. The cuvette with sample was then transferred to furnace to be heated for obtaining the absorption spectra, the heating rate is 5 °C/min until the target temperature. After the spectrum reached stable for 5 min, spectroscopic data began to be recorded. To observe the variation of spectra with temperature increasing, it grows to a new target temperature with 50 °C interval for several times and separately recorded the spectra. Every recording result repeated for five times to ensure the reliability of results.

C. Electron paramagnetic resonance

EPR spectrometer is the JES-FA200, from JEOL, Ltd. The operation temperature range is from −75 °C to 200 °C. Unlike O^{2-} and $O_2{}^{2-}$, the superoxide ($O_2{}^-$) has an unpaired electron in the antibonding orbital, so it is paramagnetic and can be probed by EPR. The 100% pure KNO_3, $NaNO_2$ and $NaNO_3$ are believed diamagnetic while the analytical grade reagents may include trace of paramagnetic impurities which may affect the background signal. In spite of this, if $O_2{}^-$ is generated during the heating process of HTS and stable after natural cooling, even at a low concentration, a sharp first-derivative EPR signal should show up which may be similar to the case of KO_2/NaO_2.

The EPR signal of powdered HTS and its components at room temperature were measured in the experiments, and a contrast experiment was carried out. We obtained the EPR results of two samples: HTS, the one being heated to the molten state and then cooled quickly to solid in sample room of EPR instrument; and a powdered mixture, with original component of 80 wt% KNO_3 and 20 wt% KO_2, which was heated at 300 °C to form a transparent yellow molten salt and then cooled down to be solid and preserved in inert atmosphere.

DOI:10.1063/1674-0068/30/cjcp1703046

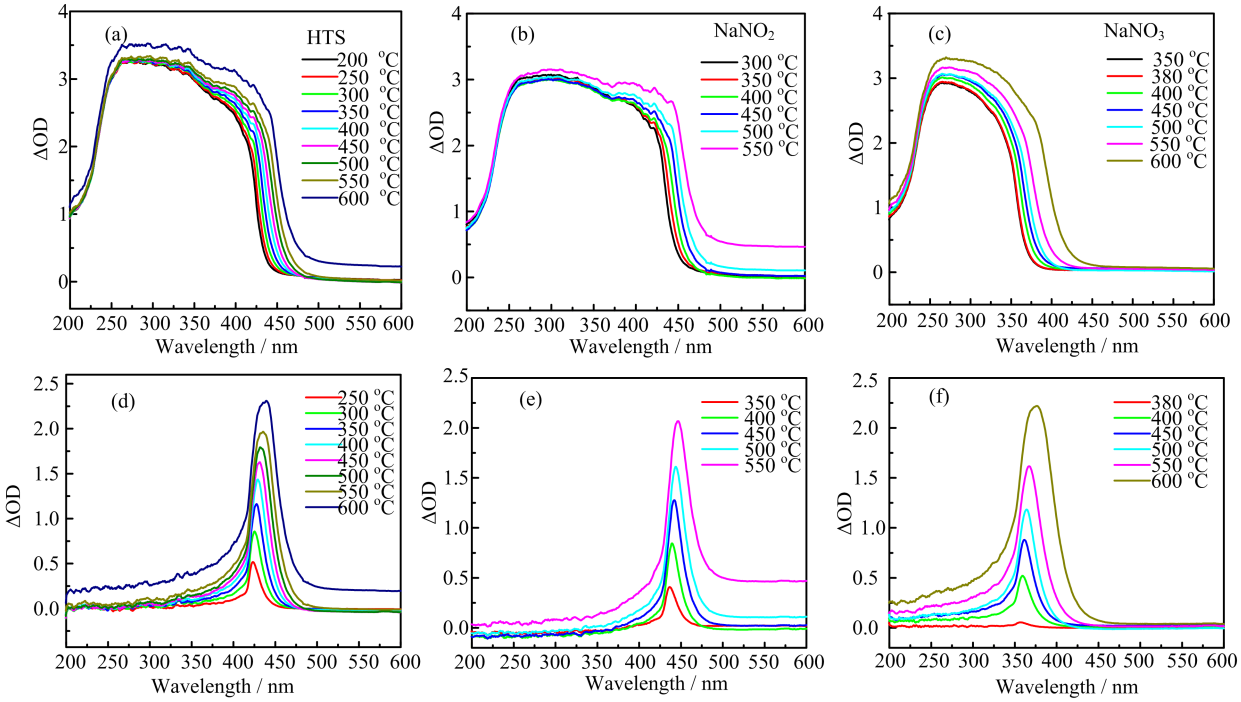

FIG. 3 UV-visible absorption spectra at different temperatures: (a) HTS, (b) $NaNO_2$, (c) $NaNO_3$. (d) Result of HTS spectra at 250−600 °C subtracting that of HTS at 200 °C. (e) Result of $NaNO_2$ spectra at 350−550 °C subtracting that of $NaNO_2$ at 300 °C. (f) Result of $NaNO_3$ spectra at 380−600 °C subtracting that of $NaNO_3$ at 200 °C.

III. RESULTS AND DISCUSSION

A. Production of superoxide (O_2^-) verified by UV-visible spectra

The absorption spectra experiment was performed on HTS, $NaNO_2$, and $NaNO_3$, which are all sealed in the cuvette and located in the inert atmosphere at the beginning. As the decomposition process of KNO_3 is very similar to $NaNO_3$, we only measured the spectra of $NaNO_3$. For HTS, it began to melt at about 150 °C in the cuvette and became totally melted and homogeneous at about 200 °C, which can be judged from the real-time spectrum. Considering the baselines obtained by measuring the empty cuvette are always stable (no baseline fluctuation with time going or temperature increasing), the homogeneity (no obvious bubbles or defects inside) of sample can be verified by the stability of the spectral curve to a certain extent, and particularly, from the absorbance (ΔOD) whose value should be very closely to zero when the curve is a horizontal line. Scattering loss can be ignored when there are no bubbles or other particles in molten salt. For the HTS sample, the measurements started at 200 °C when the HTS was completely melted, and spectra were recorded for every 50 °C intervals with the HTS heated up to 600 °C. For $NaNO_2$ and $NaNO_3$, they melted completely at 300 and 350 °C and their measurement ended at 550 and 600 °C respectively. Particularly, a spectrum of $NaNO_3$ at 380 °C was measured, because it is widely believed that $NaNO_3$ decomposes slowly to $NaNO_2$ and O_2 at 380 °C. In order to study how the spectra change with temperature increasing, a series of spectra obtained by subtracting the original spectra at the beginning tempratrue from the one at higher temperature. The results are all shown in FIG. 3.

It is found that there are no obvious gas products in HTS below 550 °C (see FIG. 3(a)), because the curves in FIG. 3(a) below and at 550°C in long wavelength region are almost the same and undistinguishable. However, the contour of spectra grows largely at 600 °C because the evident gas causes scattering loss, which means the rapid decomposition happening at this temperature. From FIG. 3 (b) and (c), the $NaNO_2$ is found much more unstable than HTS at high temperature, since the first rising curve is at about 500 °C in FIG. 3(b), lower than the one in HTS. So the experiments of HTS and $NaNO_2$ stopped at 600 and 550 °C to prevent the cuvette from high pressure and heavy corrosion [17] caused by O^{2-}, which will react with SiO_2 to generate SiO_3^{2-}.

Further evaluating FIG. 3 (a−c) shows that a dramatically absorption is located in the ultraviolet range. Due to the over-long (1 cm) optical path, the authentic absorption peak was saturated and could not be discerned. With the temperature increasing, the absorption bands of the three salts underwent red-shift, which can also be seen clearly from FIG. 3 (d−f). It is interesting to find some new absorption bands appearing when heating HTS, $NaNO_2$ and $NaNO_3$ to different temper-

DOI:10.1063/1674-0068/30/cjcp1703046

atures. Obviously, the main absorption differences in FIG. 3 (a), (b) or (c), derive not only from temperatures, but also from characteristic absorption of new species formed during the heating. Thanks to over-long optical path, the absorption bands of new species become discerned. The absorption peaks in FIG. 3 (d), (e), and (f) were denoted as A, B, and C, respectively. It can be seen from FIG. 3(d) that the absorption peak of A is situated at about 422 nm at 250 °C and it redshifts to about 439 nm at 600 °C with the intensity enhancing. From FIG. 3(e), like A, during the temperature range of 350−550 °C, the absorption peak of B red shifts from 436 nm to 446 nm. Unlike A and B, the absorption peak of C in FIG. 3(f) redshifts from 357 nm (380 °C) to 376 nm (600 °C), the peak of A is at 427 nm (350 °C) and 435 nm (550 °C). Absorption bands of A are almost the same as the one of B at the same temperature. In addition, the $NaNO_2$ was as slightly yellow as HTS when melted, so it is reasonable to believe that two new species A and B could have the same absorption band. Plausible products derived from nitrates and nitrites are speculated in the light of considering the Eq.(5) and equilibria (7)−(9), the yellow new species (A/B) are supposed to be alkali metal superoxides.

Grein and Bruna's theoretical study [37] of vertical electronic spectra of O_2^- shows that there is a calculated charge-transfer excitation $O_2^-\rightarrow Na^+/1\pi_g\rightarrow 3s$ at 2.7 eV, which will achieve the state 1^2B_1 ($2b_2\rightarrow 4a_1$). This kind of excitation corresponds to the absorption band at 463 nm, which makes the superoxide NaO_2 yellow. The color is induced owing to matter selectively absorbing photons according to modern matter structure theory [38]. When the energy gap (ΔE) between ground state and excited state is about 1.71−3.10 eV, photons with wavenumber at visible range can be absorbed to generate color. In FIG. 3 (d) and (e), the absorption bands of A and B situated at 400−490 nm represent the yellow color, which is consistent with what we observed by eyes. Bosch and Kanzig [30] also got the UV-visible absorption spectrum of solid powdered NaO_2 at room temperature by reflection method. It was found that the saturated absorption band was between 300 and 550 nm, making the maximum of absorption peak indiscernible. Mahanti and Khan [29] also thought that it is also responsible for the yellow color of the solid KO_2 by obtaining an absorption band at 350 nm by reflection at room temperature. In the molten HTS, there is trace of O_2^- but bulk of Na^+ and K^+, so the charge-transfer transitions $1\pi_g\rightarrow 3s$ or $1\pi_g\rightarrow 4s$ can still occur. While in molten $NaNO_2$, there is only charge-transfer transition $1\pi_g\rightarrow 3s$, which could also be responsible for the discrepancy of the absorption bands between HTS and $NaNO_2$ in the same temperature. With rising of temperature, the ground state energy of superoxide also grows, so the energy gap (ΔE) between ground state and excited state shrinks, which corresponds to the absorption band undergoing redshift.

Other than charge transfer, other kinds of transition happen in O_2^- itself [37]. For isolated O_2^-, with a ground state $X^2\Pi_g$ ($2\sigma_g^2 1\pi_u^4 1\pi_g^3$), the transition $1\pi_u\rightarrow 1\pi_g$ or $1\pi_g\rightarrow 2\sigma_u$ is with high ΔE corresponding to an absorption band at UV or deep UV (<200 nm) and the former with a strong absorption coefficient. In Andrews's group [28], they obtained the UV absorption spectra of alkali metal superoxides made by matrix isolation method at 17 K. An absorption band at about 250 nm was found and assigned to the transition $1\pi_u\rightarrow 1\pi_g$. However, this band will be overlapped and covered by that of $NaNO_2$ and $NaNO_3$ (at 400 °C, 244 and 242 nm respectively, see FIG. 4 (a) and (b)). Therefore, it is rational that this kind of absorption was not found in our result spectra FIG. 3 (d) and (e).

The short optical path cuvette was used to get spectra of $NaNO_2$ and $NaNO_3$ at 400 °C when they were films in cuvette (see FIG. 4 (a) and (b)). The spectrum of $NaNO_3$ has a strong band at about 242 nm and a weak band at about 300 nm at high temperature. For $NaNO_2$, they are at 244 and 354 nm. This is similar to that obtained in aqueous solution. The spectra of $NaNO_2$ and $NaNO_3$ obtained from dilute aqueous solution (0.004−1 mg/L) show a strong band at 210 and 202 nm. While in saturated aqueous solution, the absorption of two bands is saturated and shown at 354 nm ($NaNO_2$) and 300 nm ($NaNO_3$), the same as the result at high temperature.

From FIG. 3(f), a very small peak can be seen at 357 nm at 380 °C, where the slow decomposition begins, and the absorption band of C redshifts from 359 nm to 376 nm from 400 °C to 600 °C. According to the high temperature spectrum of $NaNO_2$ film at 400 °C, it is reasonable to conclude that the new species generated from $NaNO_3$ is $NaNO_2$. Previously, Young and coworkers [36] by adding NO_2^- into FLiNaK, obtained a band at 365 nm at 500 °C and assigned to NO_2^-. The band in our result of spectra at 500 °C is located at 364 nm. Consequently, our findings are in great agreement with that in the literatures, and by the way the reliability of the experimental method is verified.

Through above analysis, it can be concluded that superoxide O_2^- is generated during the decomposition of molten HTS. To be detailed, the O_2^- is mainly derived from nitrite salt. Eq.(6) is of certain possibility because a number of N_2 was found at a relatively low temperature [19].

B. Further verification of production of superoxide by EPR

In order to verify the formation of superoxide from HTS decomposition, the EPR experiments were also conducted. About 30−50 mg powdered KNO_3, $NaNO_2$, $NaNO_3$ and HTS were loaded into the quartz pipe in glovebox, then they were sealed by sealing film and measured by EPR at the room temperature. The experi-

DOI:10.1063/1674-0068/30/cjcp1703046

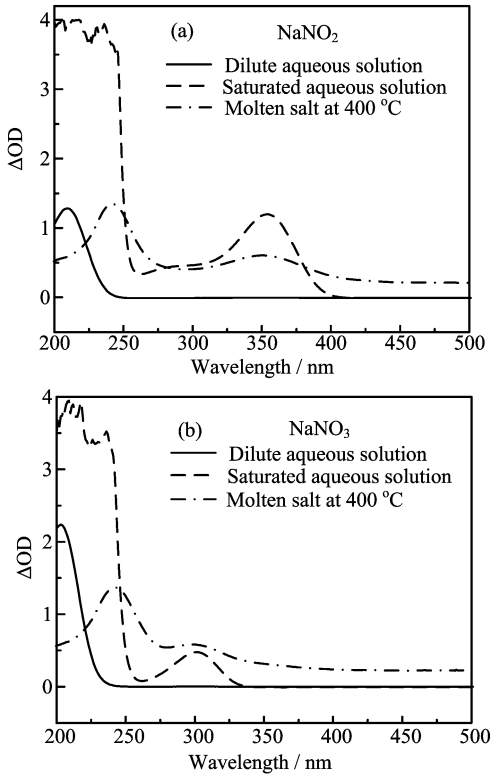

FIG. 4 (a) UV-visible spectra of $NaNO_2$ dissolved in aqueous at room temperature and the thin liquid film molten $NaNO_2$ at 400 °C. (b) UV-visible spectra of $NaNO_3$ dissolved in aqueous at room temperature and the thin liquid film molten $NaNO_3$ at 400 °C.

mental results showed no paramagnetic signal of the four samples, which means there is no superoxide in analytically pure KNO_3, $NaNO_2$, $NaNO_3$ and prepared HTS kept in glovebox for a relatively long time.

However, a sharp first-derivative signal shows up when the solid HTS which was heated to molten state, which means that the superoxide was possibly generated when heating HTS and it can be stable for a short time. Further validating the formation of superoxide, the comparison experiment was done between HTS and KNO_3 with addition of KO_2. Due to instability, KO_2 can be decomposed when heated, while it has been reported that KO_2 and KNO_3 can form eutectic structure [17, 39]. Therefore, a mixture of KNO_3 with addition of KO_2 was selected to be compared with the quickly cooled HTS after heating to molten salt. The mixture was transferred into quartz pipe and sealed, heating to 300 °C, then cooled down to room temperature. Both the cooled mixture and HTS were used to do EPR experiment. Results are displayed in FIG. 5.

A very similar signal appeared at the same magnetic field point with an average g value of 2.0169 and 2.0115 respectively, seeing FIG. 5 (a) and (b), proving the existence of O_2^- , although the backgrounds were a little different. It was indicated in Ref.[24] that superoxide

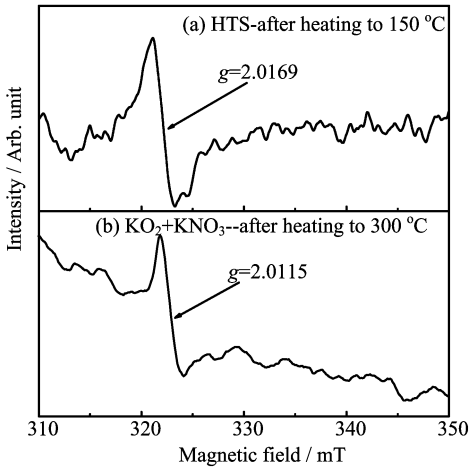

FIG. 5 The EPR signal in quickly cooled HTS and a mixture of KO_2 and KNO_3

species dissolved in various solid matrixes give origin to ESR signals presenting nonaxial tensors. So, geometry of the superoxide in molten salt is certainly in disagreement with the geometry of "free" superoxide ions. In addition, it was also showed that diatomic radicals having three electrons in a π level (such as O_2^-) usually presented a g value great than free-spin value 2.0023 [40], which were almost identical. Therefore, it is not surprising that the g value of the superoxide ion in the two samples is greater than the one of the free electron O_2^- which is unstable in $NaNO_2$, and it will further decompose into O_2^{2-}, O^{2-}, and O_2, and in addition, O_2^- will react with $NaNO_2$ to form $NaNO_3$ and O^{2-}. However, in HTS, NO_3^-, and NO_2^- account for a large proportion, and K^+ and Na^+ are able to stabilize O_2^{2-} and O_2^-, respectively, to a certain extent. Therefore, equilibriums (Eqs.(7) and (8)) [22, 24] are possible present in the HTS with certain reaction equilibrium constants, which may explain why the O_2^- in HTS is detectable by EPR.

IV. CONCLUSION

The UV-visible absorption spectra of molten HTS, $NaNO_3$ and $NaNO_2$ were gained at different temperature. Due to the strong absorption band, no obvious peak was discerned. Therefore, spectra at high temperature subtracted the spectrum at the lowest temperature, which gives a new absorption band. With temperature rising, this new band redshifts and intensity enhances. Through analysis and comparison, it is concluded that they were assigned to superoxide (O_2^-) derived from HTS decomposition. EPR results also verify this conclusion. In addition, the UV-visible result also implies that the nitrite salt is more instable than nitrate salt and easy to generate superoxide. For nitrate salt, it firstly decomposed to give nitrite salt followed by

DOI:10.1063/1674-0068/30/cjcp1703046

further decomposition to form superoxide. The yellow color can also be identified as the formation of superoxide. The study of superoxide is not only beneficial to deeply explore the decomposition mechanism of molten nitrates/nitrites salt, but also helpful to analyze the corrosion process between molten salt and metallic material in CSP system.

V. ACKNOWLEDGMENTS

This work was supported by the "Strategic Priority Research Program, TMSR" of the Chinese Academy of Sciences (No.XD02002400), the National Natural Science Foundation of China (No.51506214), the Hundred Talents Program, CAS and Shanghai Pujiang Program.

[1] H. L. Zhang, J. Baeyens, J. Degrève, and G. Cacères, Renew. Sustain. Energy Rev. **22**, 466 (2013).
[2] B. Xu, P. W. Li, and C. Chan, Appl. Energy **160**, 286 (2015).
[3] R. I. Dunn, P. J. Hearps, and M. N. Wright, Proc. IEEE **100**, 504 (2012).
[4] L. J. Wang and Q. Y. Yan, Mater. Sci. **5**, 72 (2015).
[5] D. Kearney, U. Herrmann, P. Nava, B. Kelly, R. Mahoney, J. Pacheco, R. Cable, N. Potrovitza, D. Blake, and H. Price, J. Sol. Energy Eng. **125**, 293 (2003).
[6] K. Vignarooban, X. H. Xu, A. Arvay, K. Hsu, and A. M. Kannan, Appl. Energy **146**, 383 (2015).
[7] U. Herrmann, B. Kelly, and H. Price, Energy **29**, 883 (2004).
[8] D. Kearney, B. Kelly, U. Herrmann, R. Cable, J. Pacheco, R. Mahoney, H. Price, D. Blake, P. Nava, and N. Potrovitza, Energy **29**, 861 (2004).
[9] G. J. Janz and G. N. Truong, J. Chem. Eng. Data **28**, 201 (1983).
[10] C. T. Yang, X. L. Wei, W. L. Wang, Z. H. Lin, J. Ding, Y. Wang, Q. Peng, and J. P. Yang, Appl. Energy **184**, 346 (2016).
[11] J. Alexander Jr. and S. G. Hindin, Ind. Eng. Chem. **39**, 1044 (1947).
[12] Q. Peng, X. X. Yang, J. Ding, X. L. Wei, and J. P. Yang, CIESC J. **64**, 1507 (2013).
[13] R. I. Olivares, Sol. Energy **86**, 2576 (2012).
[14] K. H. Stern, J. Phys. Chem. Ref. Data **1**, 747 (1972).
[15] C. M. Kramer, Z. A. Munir, and J. V. Volponi, Sol. Energy **29**, 437 (1982).
[16] R. N. Kust and J. D. Burke, Inorg. Nucl. Chem. Lett. **6**, 333 (1970).
[17] A. A. El Hosary, D. H. Kerridge, and A. M. Shama El Din, *Oxide Species in Molten Salts. Ionic Liquids*, D. Inman and D. G. Lovering Eds., New York: Springer, (1981).
[18] E. S. Freeman, J. Am. Chem. Soc. **79**, 838 (1957).
[19] B. D. Bond and P. W. M. Jacobs, J. Chem. Soc. A 1265 (1966).
[20] D. A. Nissen and D. E. Meeker, Inorg. Chem. **22**, 716 (1983).
[21] P. G. Zambonin and J. Jordan, J. Am. Chem. Soc. **89**, 6365 (1967).
[22] P. G. Zambonin and J. Jordan, J. Am. Chem. Soc. **91**, 2225 (1969).
[23] P. G. Zambonin, F. Paniccia, and A. Bufo, J. Phys. Chem. **76**, 422 (1972).
[24] P. G. Zambonin, Chemischer Informationsdienst **5**, 1294 (1974).
[25] M. Hayyan, M. A. Hashim, and I. M. Alnashef, Chem. Rev. **116**, 3029 (2016).
[26] D. M. Lindsay, D. R. Herschbach, and A. L. Kwiram, Chem. Phys. Lett. **25**, 175 (1974).
[27] R. R. Smardzewski and L. Andrews, J. Chem. Phys. **57**, 1327 (1972).
[28] L. Andrews, J. Mol. Spectrosc. **61**, 337 (1976).
[29] A. U. Khan and S. D. Mahanti, J. Chem. Phys. **63**, 2271 (1975).
[30] M. Bosch and W. Kanzig, Helv. Phys. Acta **48**, 743 (1975).
[31] T. Ozawa and A. Hanaki, FEBS Lett. **74**, 99 (1977).
[32] L. Andrews, J. Phys. Chem. **73**, 3922 (1969).
[33] S. Passerini and T. Mckrell, J. Nanofluids **1**, 78 (2012).
[34] J. Z. Li and P. K. Dasgupta, Rev. Sci. Instrum. **71**, 2283 (2000).
[35] X. W. Hu, Z. Sheng, B. L. Gao, Z. N. Shi, C. S. Huang, and Z. W. Wang, Metall. Anal. **34**, 32 (2014).
[36] F. L. Whiting, G. Mamantov, and J. P. Young, J. Inorg. Nucl. Chem. **34**, 2475 (1972).
[37] P. J. Bruna and F. Grein, Mol. Phys. **97**, 321 (1999).
[38] G. D. Zhou, *Inorganic Structural Chemistry*, Beijing: Science Press, (1982).
[39] X. L. Lv, *Chemistry of Inorganic Hyperoxide*, Beijing: Science Press, (1987).
[40] H. R. Zeller and W. Kanzig, Helv. Phys. Acta **40**, 845 (1967).

DOI:10.1063/1674-0068/30/cjcp1703046